

Extended Coupled Cluster approach to Twisted Graphene Layers

Ingvars Vitenburgs

*Department of Physics and Astronomy, University of Manchester, Manchester M13 9PL, UK and
Molecular Sciences Research Hub, Imperial College London, London W12 0BZ, UK*

Niels R. Walet*

Department of Physics and Astronomy, University of Manchester, Manchester M13 9PL, UK

(Dated: May 20, 2024)

A study of correlation effects in twisted bilayer graphene is presented using the extended coupled cluster method at consistent mean-field and beyond mean-field truncations. In order to describe the phase transitions in this strongly correlated system, equations and a suitable implementation is developed for the method. Combining modern tensor contraction techniques with singular value decomposition, the correlation effects are successfully described in a qualitative manner, with the majority of both short-range and long-range Coulomb interactions included. The superconducting gap is found to peak at an angle $\theta_c = 1.00^\circ$ with a BCS value for the critical temperature of $T_c^{\text{BCS}} = 0.8\text{K}$ matching closely with experiment. Additionally, a homogeneous (s-wave) gap is found. While the simulations are somewhat limited by the truncations used, nevertheless, a strong candidate for the mechanism behind superconductive phases in twisted bilayer graphene is presented.

I. INTRODUCTION

The mechanism that gives rise to the recently discovered [1, 2] superconducting and insulating phases in twisted bilayer graphene (TBG), is of great interest. Theoretical modelling has led to several suggestions for the mechanisms behind these phenomena including long-range electron-electron interactions at Hartree-Fock level, Umklapp scattering and electron-phonon interactions [3, 4], but, unfortunately, have yet to yield a fully successful description due to being orders of magnitude off experimental values [2, 5] of the critical temperature. Additionally, there have been many studies [6–14] connecting various symmetries, as well as small amounts of strain, with the behaviour of TBG, thus obtaining various predictions. Nevertheless, quite a few previous Hartree-Fock studies suggest [15–20] that electrostatic interactions play a leading role in this system and hence correlation effects could be the key to understanding the states, with some initial studies already being partially conducted [21].

One powerful approach, that incorporates the Hartree-Fock equations and can be used to systematically include additional correlations, is the extended coupled cluster (ECC) method [22–27]. In this work, an efficient numerical procedure is developed to implement such calculations for graphene. All coupled cluster methods are formulated in a wave-function approach, with an exponential of a set of independent excitations acting on a suitable reference state. These excitation operators are usually denoted in terms of single, double, triple, etc. correlated excitations. The reason coupled clusters are efficient to implement and their key defining feature is that the bra and ket states are not the usual Hermitian conjugates. However, that can be of benefit as well.

In the case of graphene systems, the natural choice for the reference state is the non-interacting half-filled Fermi sea, which means that excitations are labelled by the number of particle-hole states. This can be most easily done by introducing the particle and hole operators to simplify the algebra. It is known (and relatively easy to show) that the ECC singles approach with only one-particle-one-hole excitations is equivalent to the unrestricted Hartree-Fock approximation - this is not the case for the more commonly used normal coupled cluster (NCC) method [28], which has also been applied to graphene [21].

At the level of the singles truncation, it is most natural in the particle hole-formalism to include all operators containing two creation operators states. This describes one-particle-one-hole, two-particle and two-hole excitations, which thus contain the description of pair-correlations fully equivalent to the Hartree-Fock-Bogoliubov formalism - without any assumption about the nature of the pairing gap. Due to the equivalence to the mean-field methods, unlike the NCC method, ECC can also be used to describe phase transitions, even if the reference state does not describe the new phase. This is especially important for strongly correlated systems with multiple phases, such as TBG, since there is no requirement for the reference state to change from phase to phase. Finally, the effect of partial filling due to a bias potential applied to graphene can be included in the usual way using a chemical potential.

One of the great advantages of coupled cluster methods over other approaches is the finite polynomial nature of energy expressions and other expectation values. These can be seen as tensor contractions, so modern techniques developed for machine learning can be used to perform the search for extrema, using tensor manipulations and singular value decomposition. This means that it is straightforward to efficiently implement such tasks on GPUs. The main goal of this paper is therefore

* niels.walet@manchester.ac.uk

to show that the ECC method can be used to describe TBG, minimise the energy and describe correlations beyond mean-field truncation, while dealing with pairing and Hartree-Fock correlations on an equal footing.

The paper is organised as follows: In Section II a very minimal definition of the ECC method and the equations used is given, with details relegated to appendices A and B. Then, in Section III this approach is validated with monolayer graphene by analysing the band structure and Fermi level away from half-filling to obtain confidence in the qualitative accuracy of the developed method and its implementation. In Section IV superconductivity of TBG near the first magic angle is studied. Further steps are discussed in Section V.

II. EXTENDED COUPLED CLUSTER

The ECC method [22–25] is a quantum many-body method that formally combines a mean-field description at singles truncation with correlation effects at higher truncation levels. Hence, it is perfect for describing strongly correlated systems with phase transitions. Given the Hamiltonian \hat{H} , its expectation value is given by

$$\langle \hat{H} \rangle = \langle - | e^{\hat{T}'} e^{-\hat{T}} \hat{H} e^{\hat{T}} | - \rangle. \quad (1)$$

Here, the reference state $| - \rangle$ is the half-filled one that describes the non-interacting ground state at charge neutrality. The operators are expressed in the particle-hole basis, which gives a natural normal ordering relative to $| - \rangle$.

In the ECC singles and doubles (ECCSD) truncation, the excitation operators \hat{T} and \hat{T}' are expanded to fourth order, using single-particle operators, to produce

$$\begin{aligned} \hat{T} &= \frac{1}{2!} t_{ij} \hat{d}_i^\dagger \hat{d}_j^\dagger + \frac{1}{4!} t_{ijkl} \hat{d}_i^\dagger \hat{d}_j^\dagger \hat{d}_k^\dagger \hat{d}_l^\dagger, \\ \hat{T}' &= \frac{1}{2!} t'_{ij} \hat{d}_i \hat{d}_j + \frac{1}{4!} t'_{ijkl} \hat{d}_i \hat{d}_j \hat{d}_k \hat{d}_l. \end{aligned} \quad (2)$$

Only even powers of the operators are kept in order to preserve fermion parity, and the indices of the tensors represent the quantum numbers of the system. Eq. (1) is similar to the more widely used NCC expression [28] which can be understood as a subset of this method, obtained by expanding $e^{\hat{T}'}$ to first order in \hat{T}' . In standard coupled-cluster terminology, Eq. (2) is the extended coupled cluster method at doubles truncation. The resulting equations for energy and particle number can be found in Appendix A. These were derived with some help of the Sympy [29] package.

In order to change the filling, a chemical potential is added, by minimising the grand potential [30]

$$\Omega = \langle \hat{H} - \mu(\hat{N} - N_0) \rangle. \quad (3)$$

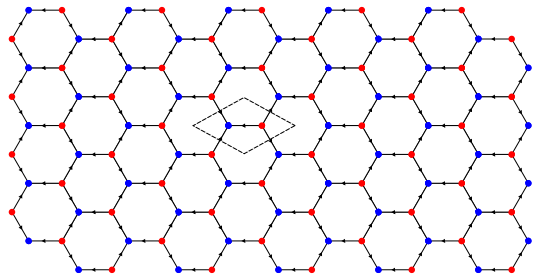


FIG. 1. Geometric structure of monolayer graphene. The system is assumed to be described by a nearest-neighbour hopping between the blue and red sites. The dashed region represents the unit cell.

However, to have numerical stability, a quadratic constraint is used instead,

$$\Omega' = \langle \hat{H} \rangle + \gamma(\langle \hat{N} \rangle - N_0)^2, \quad (4)$$

Here γ is a suitably chosen parameter and the desired filling can be adjusted by varying N_0 . The chemical potential can then be calculated at the unconstrained minimum of Ω' ,

$$\mu = -2\gamma(\langle \hat{N} \rangle - N_0). \quad (5)$$

In order to describe single-particle excited state energies ϵ , an eigenvalue problem for momentum conserving states can be formed via

$$\begin{aligned} \langle \hat{O}_{ij} \rangle &= \langle - | \hat{d}_{\mathbf{k},i} e^{\hat{T}'} e^{-\hat{T}} \hat{H} e^{\hat{T}} \hat{d}_{\mathbf{k},j}^\dagger | - \rangle, \\ \hat{O}\Psi &= \epsilon\Psi. \end{aligned} \quad (6)$$

This is similar to the equation-of-motion framework at singles truncation. The resulting equation can also be found in Appendix A.

Finally, the automatic differentiation functionality in PyTorch [31, 32] was used in tandem with tensor contractions using the "einsum" function to numerically minimize Eq. (4) thus obtaining the ground state energy.

III. MONOLAYER GRAPHENE

In order to validate the newly developed ECCSD implementation, it was tested on a simple model of monolayer graphene [33]. In the non-interacting case, this is described by a simple nearest-neighbour hopping model between the blue and red sites, displayed in Fig. 1 below. This describes the standard semimetallic spectrum of graphene. A Coulomb interaction between electrons is then added and, due to the use of periodic boundary conditions, the Ewald summation [34, 35] technique in combination with the Widom insertion method [36] is

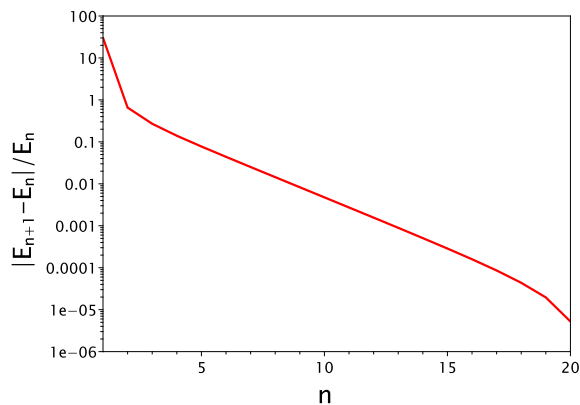


FIG. 2. Convergence of the ECCSD simulation energy for monolayer graphene as a function of the simulation (stochastic gradient descent solver) step n . The particle number was observed to converge in a very similar fashion.

used as well. A simple Monkhorst-Pack grid [37, 38] was implemented for sampling the lattice.

A ECCSD simulation was run for this system, obtaining polynomial convergence, as displayed in Fig. 2 below. It was terminated once the relative difference between runs of the stochastic gradient descent solver reached 10^{-6} . This is because of the floating point number precision used in order to lower the computational cost.

Generally, to extract asymptotic values of any observable, with respect to convergence parameters, extrapolation was performed throughout this study using curves of the form

$$O(n) = O_\infty + \frac{A}{B^n}. \quad (7)$$

In all further simulations, it was required that the n for the final convergence step was large enough so that the values of $O(n)$ were within 10% of the asymptotic value O_∞ . This ensures that converged results could be reliably extracted.

An identical shift of 25 meV, but opposite sign, of the excited state energy was obtained at the Dirac point for both bands at $N_0 = \pm 1$ fillings. A further calculation of the chemical potential yielded a Fermi level of 110 meV. Correlation effects can now be studied by comparing simulations at singles and doubles truncation. While there is negligible impact on the spectrum (changes of the order of one part in a thousand) at $N_0 = +1$ filling, the Fermi level increases by 40 meV when correlation effects were taken into account. Thus, correlations may have a quite significant impact on the electrical conductivity in monolayer graphene.

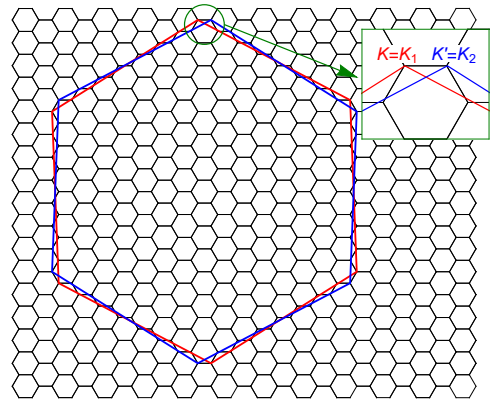


FIG. 3. Reciprocal lattice of twisted bilayer graphene. The black hexagons are the TBG unit cells, while the blue and red hexagons are the reciprocal unit cells for each graphene layer. The inset shows that the superlattice K and K' points are the individual K points of the twisted graphene lattices.

IV. SUPERCONDUCTIVITY IN TWISTED BILAYER GRAPHENE

Having gained confidence in the newly developed method, it is applied to a system of interest - twisted bilayer graphene - to potentially obtain a qualitative description of the reported superconductivity.

Even though in principle an atomic basis can be used, the dimensionality of the problem explodes, making it impossible to implement on relatively simple computational resources. That is one of the reasons TBG is widely modelled by the Bistritzer-MacDonald (BM) model [39] which is a low energy continuum description, suitable for small twist angles. The expansion is based on the continuum graphene spectrum at the relevant Dirac points in each layer, as well as a lowest-harmonic expansion of the hopping between the layers, displayed in Fig. 3.

The BM model is defined by a block Hamiltonian

$$\hat{H} = \begin{pmatrix} H_1 & U \\ U^\dagger & H_2 \end{pmatrix}_{ij} \hat{d}_i^\dagger \hat{d}_j. \quad (8)$$

Here, H_1 and H_2 represent the continuum graphene Hamiltonian in each of the layers, while U describes the hopping. To include the majority of the contributing processes into this model, the Dirac point, as well as its 6 nearest neighbours, is taken into account [15] together with couplings from each one of them to the three nearest ones in the second layer [40]. This corresponds to $\sim 80\%$ of the total short-range interactions. Further, a metallic gate potential [41] is used to model the enclosure of TBG between two layers of hexagonal boron nitride. It is characterised by a gate spacing parameter D via

$$V(q) \propto \frac{\tanh(Dq)}{q}. \quad (9)$$

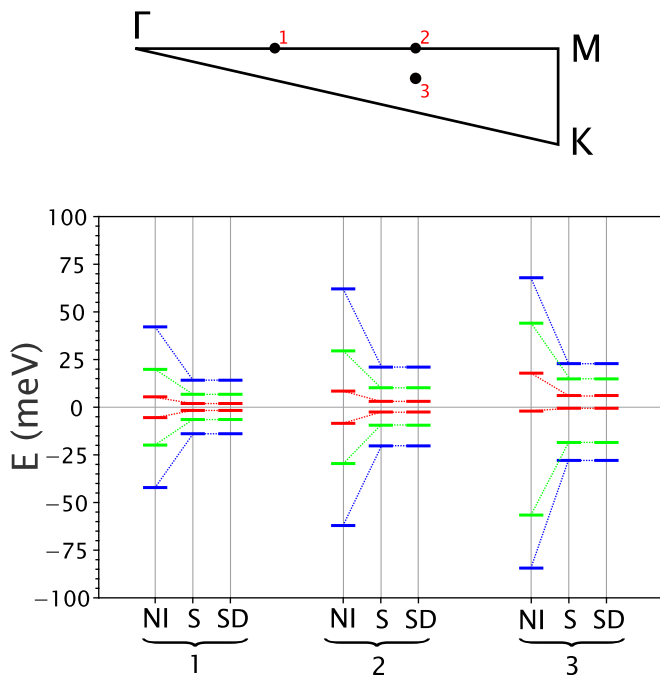


FIG. 4. The band structure of twisted bilayer graphene, sampled at three points - two points equidistant on the $K - M$ line and one in the middle of the $\Gamma - K - M$ zone, as shown at the top of the figure. For each point, the non-interacting case (NI) and the ECCS and ECCSD coupled cluster truncations are shown.

The ECCSD simulations were initially run at different truncation levels for a filling of $N_0 = +2$, which has been reported to exhibit potential for insulating to conductive phase transition [17]. A similar convergence to monolayer graphene was obtained of the stochastic gradient descent solver, with around twice as many steps required to reach the relative energy change threshold of 10^{-6} . Because of the significantly smaller first Brillouin zone, in comparison with monolayer graphene, a smaller number of sampling points were expected to be necessary for convergence. This proved to be true, after analysing Eq. (7) type fitted curves, as discussed previously, with only four points required for a qualitative description.

Due to computational cost, only three points were sampled via the Monkhorst-Pack grid at this time - two equidistant ones on the $K - M$ momentum line and one in the middle of the $\Gamma - K - M$ zone. Nevertheless, as displayed in Fig. 4 above, this gave a qualitative description of the mean-field effects, which matched previous work [16, 17] in that electrostatic interactions have a leading role in the band structure. Furthermore, the effect of correlations was negligible, with a relative contribution of $\sim 10^{-2}$ to the band structure, which is hardly expected to change by an additional sampling point. A further ECCS calculation of the chemical potential yielded a Fermi level of 25 meV thus signifying occupation of these bands and further matching previous studies on the role of the electrostatic interactions on conductivity in TBG

and thus giving additional confidence in the current ECC implementation.

One of the main limitations of these calculations is the amount of storage needed for four-index tensors (t_{ijkl} , t'_{ijkl} , V_{ijkl}). Hence, the rank-4 tensors, appearing in the ECCSD equations, were decomposed [42] into rank-3 ones using momentum conservation. This significantly lowers the computational cost and is represented by, e.g.,

$$t_{ijkl} = t_{ij}^a t_{kl}^a - t_{ik}^a t_{jl}^a + t_{il}^a t_{kj}^a. \quad (10)$$

$$V_{pqrs} = \bar{V}_{pq}^a V_{rs}^a.$$

Rewriting the ECCSD equations at singles level is trivial, but the doubles level requires further simplification, and the resulting equations can be found in Appendix B.

Note that further SVD was performed to significantly lower the summation range of the third - a - index. The eigenvectors, corresponding to the largest eigenvalues of $E_{ab} = \bar{V}_{ij}^a V_{ij}^b$, are used to construct a transformation matrix U_{ij} to compute the decomposed $\tilde{V}_{ij}^a = U_q^a V_{ij}^q$.

Hence, the majority of the contributing terms can be included, based on a truncation on singular values. The 16 largest singular values and associated eigenvectors of the potential V_{pq}^a were used, corresponding to $\sim 70\%$ of the long-range interactions. The same cut-off was used for t_{ij}^a , as well, since it is expected to have essentially equivalent dynamics in a numerical sense. This leads to a significant performance boost, especially since the simulations now fit on an NVIDIA 80GB A100 graphics processing unit, designed for fast tensor calculations. Nevertheless, the limited amount of RAM in commercially available GPUs is still the main reason for not including contributions corresponding to smaller singular energies.

This allows for describing superconductivity via the superconducting gap [43], defined as

$$\Delta_{\mathbf{k}} = - \sum_{\mathbf{k}_1} V_{\mathbf{k}, \mathbf{k}_1} \langle \hat{d}_{\mathbf{k}_1, \uparrow} \hat{d}_{-\mathbf{k}_1, \downarrow} \rangle. \quad (11)$$

The tensor contractions for this expectation value can be found in Appendix A. The implementation for measuring this observable requires introducing spin and momenta of opposite sign, totalling ~ 1000 sites for a qualitative description with four sampled points.

An initial ECCSD simulation showed that the addition of correlation effects via doubles yields an increase of the Fermi level by 7 meV, thus having relatively significant impact on the band energy gaps and electrical conductivity. The peak of the superconducting gap energy was found at a twist angle of $\theta_c = 1.00^\circ$. The k -dependent gap at this angle and filling $N_0 = +2$ is shown in Fig. 5. As previously discussed, the current approach makes no assumption about the nature of the superconducting gap, but the results clearly point at s -wave superconductivity, which seems to contradict suggestions from previous studies [5, 44]. While rotational symmetry dominates,

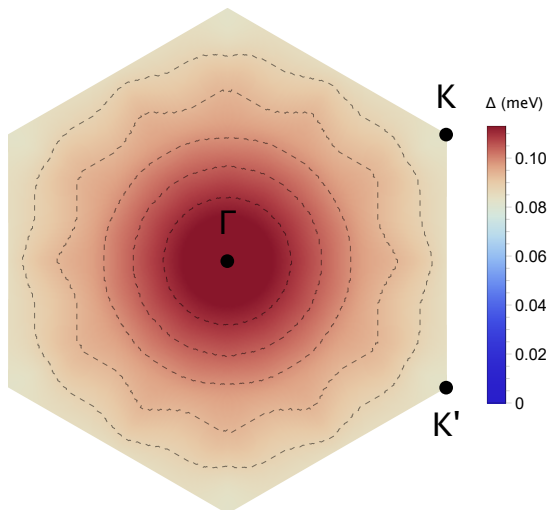


FIG. 5. The momentum dependent superconducting gap of twisted bilayer graphene for filling $N_0 = +2$ and twist angle $\theta = 1.00^\circ$.

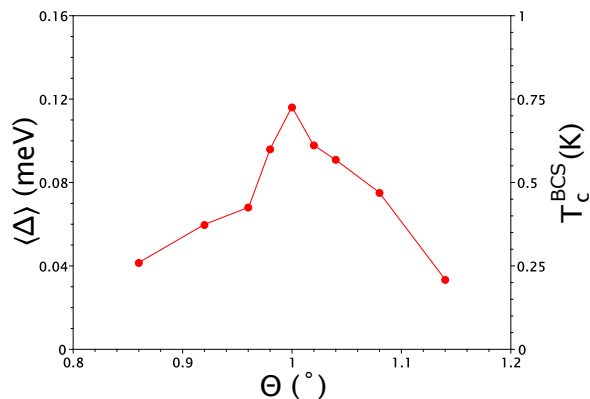


FIG. 6. The mean superconducting gap over the first Brillouin zone (left scale) and the BCS estimate of the critical temperature (right scale) as a function of the twist angle of twisted bilayer graphene for a filling $N_0 = +2$.

higher order harmonics are observed in the superconducting gap across the first Brillouin zone as well.

Furthermore, since the superconducting gap is approximately uniform with respect to the momentum, it seems sensible to assume Bardeen–Cooper–Schrieffer (BCS) theory applies and, hence, the zero-temperature gap can be related to the critical temperature via $\langle \Delta \rangle \approx 1.78 k_B T_c^{\text{BCS}}$. This corresponds to the temperature where superconductivity vanishes. A peak of the gap value and thus the critical temperature was obtained at an angle $\theta_c = 1.00^\circ$ with a value of $T_c^{\text{BCS}} = 0.8K$. The distribution of the average gap energies, with respect to the twist angle, is displayed in Fig. 6 above, along with the respective critical temperatures.

Looking at the form of ECCSD equations, it can be

seen that a non-zero superconducting gap is mathematically not possible via mean-field theory - only by accounting correlation effects via doubles and higher truncation levels - since no singles amplitudes are present. By further looking at the particle number equation, it is easy to see that at $N_0 = 0$ filling - charge neutrality - the equations can be solved by null amplitudes and hence the superconducting gap vanishes. It was found that an integer increase or decrease of the filling from $N_0 = +2$ yielded an increase or decrease of the superconducting gap by $\sim 10\%$ respectively.

The values obtained above are quantitatively very close to the experimental ones [2, 5], $\theta \sim 1.1^\circ$ and $T_c \sim 1K$. It is believed that inclusion of more terms in the BM model, tensor SVD decomposition and ECC truncation will yield a quantitative description, although this would come at a substantial computational cost.

V. CONCLUSIONS

It has been shown that one can study correlation effects in TBG using the coupled cluster method. This was done within the BM model with an added double metallic gate potential to account for electrostatic interactions in an experimental setting, assumed TBG is sandwiched between hBN layers. Furthermore, equations were derived for the ECCSD method, suitable for study of phase transitions in strongly correlated systems. The spectrum of monolayer graphene is successfully described to gain confidence in the method and its implementation.

For TBG, simulations at singles truncation agree with previous Hartree-Fock studies in that electrostatic effects are the leading contribution to the conductivity, because of the significant narrowing of the gaps in the band structure and impact on the Fermi level. Correlation effects at doubles truncation show insignificant contributions to the band structure, but a relatively significant increase of the Fermi level.

By the use of tensor decomposition and SVD, it was made possible to qualitatively simulate the superconducting gap energies and hence estimate the critical temperature and angle at which the electrical resistivity disappears. The obtained values of $\theta_c = 1.00^\circ$ and $T_c = 0.8K$ matched the experimental values closely at a qualitative level. Additionally, s-wave symmetry was found to be present in TBG, contrary to some suggestions in past research. Hence, this study presents a serious contender for the mechanism behind superconductive phases in TBG, in contrast to most previous studies.

VI. ACKNOWLEDGEMENTS

I.V. is supported by a Royal Society doctoral studentship via grant URF-R1-191292. N.R.W. is supported by a Science and Technology Facilities Council grant

ST/V001116/1. The authors acknowledge access to com-

puting resources provided by the Imperial College Research Computing Service.

-
- [1] Y. Cao, V. Fatemi, A. Demir, S. Fang, S. L. Tomarken, J. Y. Luo, J. D. Sanchez-Yamagishi, K. Watanabe, T. Taniguchi, E. Kaxiras, R. C. Ashoori, and P. Jarillo-Herrero, Correlated insulator behaviour at half-filling in magic-angle graphene superlattices, *Nature* **556**, 80 (2018).
- [2] Y. Cao, V. Fatemi, S. Fang, K. Watanabe, T. Taniguchi, E. Kaxiras, and P. Jarillo-Herrero, Unconventional superconductivity in magic-angle graphene superlattices, *Nature* **556**, 43 (2018).
- [3] T. Cea and F. Guinea, Coulomb interaction, phonons, and superconductivity in twisted bilayer graphene, *Proceedings of the National Academy of Sciences of the United States of America* **118** (2021).
- [4] C. K. Lewandowski, S. Nadj-Perge, and D. Chowdhury, Does filling-dependent band renormalization aid pairing in twisted bilayer graphene?, *npj Quantum Materials* **6**, 1 (2021).
- [5] M. Oh, K. P. Nuckolls, D. Wong, R. L. Lee, X. Liu, K. Watanabe, T. Taniguchi, and A. M. Yazdani, Evidence for unconventional superconductivity in twisted bilayer graphene, *Nature* **600**, 240 (2021).
- [6] Y. Zhang, K. Jiang, Z. Wang, and F.-C. Zhang, Correlated insulating phases of twisted bilayer graphene at commensurate filling fractions: A hartree-fock study, *Physical Review B* **102**, 035136 (2020).
- [7] M. Xie and A. H. MacDonald, Nature of the correlated insulator states in twisted bilayer graphene, *Physical Review Letters* **124**, 097601 (2020).
- [8] N. Bultinck, E. Khalaf, S. Liu, S. Chatterjee, A. Vishwanath, and M. P. Zaletel, Ground state and hidden symmetry of magic-angle graphene at even integer filling, *Physical Review X* **10**, 031034 (2020).
- [9] J. Liu and X. Dai, Theories for the correlated insulating states and quantum anomalous hall effect phenomena in twisted bilayer graphene, *Physical Review B* **103**, 035427 (2021).
- [10] J. Y. Lee, E. Khalaf, S. Liu, X. Liu, Z. Hao, P. Kim, and A. Vishwanath, Theory of correlated insulating behaviour and spin-triplet superconductivity in twisted double bilayer graphene, *Nature Communications* **10** (2019).
- [11] S. Liu, E. Khalaf, J. Y. Lee, and A. Vishwanath, Nematic topological semimetal and insulator in magic-angle bilayer graphene at charge neutrality, *Physical Review Research* (2019).
- [12] E. Khalaf, N. Bultinck, A. Vishwanath, and M. P. Zaletel, Soft modes in magic angle twisted bilayer graphene, *arXiv: Strongly Correlated Electrons* (2020).
- [13] D. E. Parker, T. Soejima, J. Hauschild, M. P. Zaletel, and N. Bultinck, Strain-induced quantum phase transitions in magic-angle graphene., *Physical review letters* **127** **2**, 027601 (2020).
- [14] G. Wagner, Y. H. Kwan, N. Bultinck, S. H. Simon, and S. A. Parameswaran, Global phase diagram of the normal state of twisted bilayer graphene., *Physical review letters* **128** **15**, 156401 (2021).
- [15] F. Guinea and N. R. Walet, Electrostatic effects, band distortions, and superconductivity in twisted graphene bilayers, *Proceedings of the National Academy of Sciences of the United States of America* **115**, 13174 (2018).
- [16] T. Cea, N. R. Walet, and F. Guinea, Electronic band structure and pinning of fermi energy to van hove singularities in twisted bilayer graphene: A self-consistent approach, *Physical Review B* (2019).
- [17] T. Cea, P. A. Pantaleón, N. R. Walet, and F. Guinea, Electrostatic interactions in twisted bilayer graphene, *Nano Materials Science* (2021).
- [18] P. A. Pantaleón, T. Cea, R. Brown, N. R. Walet, and F. Guinea, Narrow bands, electrostatic interactions and band topology in graphene stacks, *2D Materials* **8** (2020).
- [19] T. Cea and F. Guinea, Band structure and insulating states driven by coulomb interaction in twisted bilayer graphene, *Physical Review B* **102**, 045107 (2020).
- [20] A. Jimeno-Pozo, Z. A. H. Goodwin, P. A. Pantaleón, V. Vitale, L. Klebl, D. M. Kennes, A. A. Mostofi, J. Lischner, and F. Guinea, Short versus long range exchange interactions in twisted bilayer graphene, *Advanced Physics Research* **2** (2023).
- [21] F. M. Faulstich, K. D. Stubbs, Q. Zhu, T. Soejima, R. Dilip, H. Zhai, R. Kim, M. P. Zaletel, G. K.-L. Chan, and L. Lin, Interacting models for twisted bilayer graphene: A quantum chemistry approach, *Physical Review B* (2022).
- [22] J. Arponen, Variational principles and linked-cluster expansions for static and dynamic many-body problems, *Annals of Physics* **151**, 311 (1983).
- [23] J. S. Arponen, R. F. Bishop, and E. Pajanne, Extended coupled-cluster method. i. generalized coherent bosonization as a mapping of quantum theory into classical hamiltonian mechanics., *Physical review. A, General physics* **36** **6**, 2519 (1987).
- [24] J. S. Arponen, R. F. Bishop, and E. Pajanne, Extended coupled-cluster method. ii. excited states and generalized random-phase approximation., *Physical review. A, General physics* **36** **6**, 2539 (1987).
- [25] Arponen, Bishop, Pajanne, and Robinson, Extended coupled-cluster method. iii. zero-temperature hydrodynamics of a condensed bose fluid., *Physical review. A, General physics* **37** **4**, 1065 (1988).
- [26] Robinson, Bishop, and Arponen, Extended coupled-cluster method. iv. an excitation energy functional and applications to the lipkin model., *Physical review. A, General physics* **40** **8**, 4256 (1989).
- [27] A. Laestadius and S. Kvaal, Analysis of the extended coupled-cluster method in quantum chemistry, *SIAM J. Numer. Anal.* **56**, 660 (2017).
- [28] I. Shavitt and R. J. Bartlett, *Many-Body Methods in Chemistry and Physics: MBPT and Coupled-Cluster Theory* (Cambridge University Press, 2009).
- [29] A. Meurer, C. P. Smith, M. Paprocki, O. Certik, S. B. Kirpichev, M. Rocklin, A. Kumar, S. Ivanov, J. K. Moore, S. Singh, T. Rathnayake, S. Vig, B. E. Granger, R. P. Muller, F. Bonazzi, H. Gupta, S. Vats, F. Johans-

- son, F. Pedregosa, M. J. Curry, A. R. Terrel, S. Roucka, A. Saboo, I. Fernando, S. Kulal, R. Cimrman, and A. M. Scopatz, *Sympy: Symbolic computing in python*, PeerJ Prepr. **4**, e2083 (2017).
- [30] A. Fetter and J. Walecka, *Quantum Theory of Many-Particle Systems* (McGraw-Hill Book Co., New York, 1971).
- [31] A. Paszke, S. Gross, F. Massa, A. Lerer, J. Bradbury, G. Chanan, T. Killeen, Z. Lin, N. Gimelshein, L. Antiga, A. Desmaison, A. Köpf, E. Yang, Z. DeVito, M. Raison, A. Tejani, S. Chilamkurthy, B. Steiner, L. Fang, J. Bai, and S. Chintala, *Pytorch: An imperative style, high-performance deep learning library*, in *Neural Information Processing Systems* (2019).
- [32] A. Paszke, S. Gross, S. Chintala, G. Chanan, E. Yang, Z. DeVito, Z. Lin, A. Desmaison, L. Antiga, and A. Lerer, *Automatic differentiation in pytorch* (2017).
- [33] A. H. C. Neto, F. Guinea, N. M. R. Peres, K. S. Novoselov, and A. K. Geim, *The electronic properties of graphene*, *Reviews of Modern Physics* **81**, 109 (2007).
- [34] P. P. Ewald, *Die berechnung optischer und elektrostatischer gitterpotentiale*, *Annalen der Physik* **369**, 253 (1921).
- [35] F. E. Harris, *Ewald summations in systems with two-dimensional periodicity*, *International Journal of Quantum Chemistry* **68**, 385 (1998).
- [36] A. Bakhshandeh and Y. Levin, *Widom insertion method in simulations with ewald summation.*, *The Journal of chemical physics* **156** **13**, 134110 (2022).
- [37] H. J. Monkhorst and J. D. Pack, *Special points for brillouin-zone integrations*, *Physical Review B* **13**, 5188 (1976).
- [38] J. D. Pack and H. J. Monkhorst, "special points for brillouin-zone integrations" — a reply, *Physical Review B* **16**, 1748 (1977).
- [39] R. Bistritzer and A. H. Macdonald, *Moire bands in twisted double-layer graphene*, *Proceedings of the National Academy of Sciences* **108**, 12233 (2010).
- [40] F. Guinea and N. R. Walet, *Continuum models for twisted bilayer graphene: Effect of lattice deformation and hopping parameters*, *Physical Review B* (2019).
- [41] Z. A. H. Goodwin, V. Vitale, F. Corsetti, D. K. Efetov, A. A. Mostofi, and J. Lischner, *Critical role of device geometry for the phase diagram of twisted bilayer graphene*, *Physical Review B* (2019).
- [42] F. Hummel, T. Tsatsoulis, and A. Gruneis, *Low rank factorization of the coulomb integrals for periodic coupled cluster theory.*, *The Journal of chemical physics* **146** **12**, 124105 (2016).
- [43] J. F. Annett, *Superconductivity, superfluids, and condensates* (Oxford University Press, 2004).
- [44] E. Lake, A. S. Patri, and T. Senthil, *Pairing symmetry of twisted bilayer graphene: A phenomenological synthesis*, *Physical Review B* (2022).

Appendix A: Extended Coupled Cluster Doubles Equations

The Hamiltonian can be expressed in second-quantised form as

$$\hat{H} = \epsilon_{ij} \hat{d}_i^\dagger \hat{d}_j + \frac{1}{2} V_{ijkl} \hat{d}_i^\dagger \hat{d}_j^\dagger \hat{d}_k \hat{d}_l. \quad (\text{A1})$$

Here ϵ_{ij} is a Hermitian matrix and V_{ijkl} is pairwise antisymmetric. The energy equation for extended coupled cluster at doubles truncation is then found

$$\begin{aligned} \langle - | e^{\hat{T}'} e^{-\hat{T}} \hat{H} e^{\hat{T}} | - \rangle = & \epsilon_{ik} t_{jk} t'_{ij} + \frac{1}{2} V_{ijkl} t'_{ij} t_{kl} - \frac{1}{2} V_{ikkl} t'_{ij} t_{jl} + \frac{1}{2} V_{ijmnt} t_{km} t_{ln} (t'_{ij} t'_{kl} - 2t'_{ik} t'_{jl} + t'_{ijkl}) \\ & + \frac{1}{12} V_{imnnt} t_{jkl} t'_{ij} t_{kl} + \frac{1}{4} V_{ijmnt} t_{klmn} (2t'_{ik} t'_{jl} - t'_{ijkl}) - \frac{1}{6} \epsilon_{im} t_{jklm} t'_{ijkl} \\ & + \frac{1}{6} V_{ijopt} t_{kotl} t_{mnp} (2t'_{ik} t'_{jlmn} + 6t'_{im} t'_{jkl} + 3t'_{km} t'_{jln} - t'_{ij} t'_{klmn} + 6t'_{il} t'_{jm} t'_{kn}) \\ & + \frac{1}{72} V_{ijrst} t_{klm} r t_{nops} (6t'_{ijkl} t'_{mnop} + 9t'_{ijkn} t'_{lmop} - 18t'_{imop} t'_{jkl} - 2t'_{iklm} t'_{jnop} \\ & + 9t'_{ij} t'_{kn} t'_{lmop} + 12t'_{ik} t'_{jm} t'_{lnop} + 18t'_{ik} t'_{jo} t'_{lmnp} + 72t'_{ik} t'_{ln} t'_{jmop} - 18t'_{lp} t'_{mn} t'_{ijk} \\ & + 6t'_{ij} t'_{kn} t'_{lp} t'_{mo} + 36t'_{ik} t'_{jn} t'_{lo} t'_{mp}). \end{aligned} \quad (\text{A2})$$

The amplitude tensors t are fully antisymmetric. Further, the particle number is derived to be

$$\langle \hat{N} \rangle = \lambda_i \langle - | e^{\hat{T}'} e^{-\hat{T}} \hat{d}_i^\dagger \hat{d}_i e^{\hat{T}} | - \rangle = \lambda_i (-t_{ij} t'_{ij} + \frac{1}{6} t_{ijkl} t'_{ijkl}). \quad (\text{A3})$$

Here λ_i is -1 for hole states and $+1$ for particles. Finally, the expression for matrix elements, used to calculate excited state energies, is

$$\begin{aligned} \langle - | \hat{d}_x e^{\hat{T}'} e^{-\hat{T}} \hat{H} e^{\hat{T}} \hat{d}_y^\dagger | - \rangle = & \epsilon_{xy} + \delta_{xy} (E + V_{xyi}) - 2V_{xijm} t_{km} t'_{ik} - V_{ijym} t_{xm} t'_{ij} + \\ & + \frac{1}{2} V_{ijyo} t_{xklo} (2t'_{il} t'_{jk} + t'_{ijkl}) + \frac{1}{3} V_{xyio} t_{klmo} t'_{iklm}. \end{aligned} \quad (\text{A4})$$

Finally, the expectation value required for calculating the superconducting gap is derived to be

$$\langle \hat{d}_x \hat{d}_y \rangle = \langle - | e^{\hat{T}'} e^{-\hat{T}} \hat{d}_x \hat{d}_y e^{\hat{T}} | - \rangle = \frac{1}{8} t_{xijk} t_{ylmn} (t'_{in} t'_{jl} t'_{km} - t'_{il} t'_{jkmn}). \quad (\text{A5})$$

Appendix B: Singular value expansion and ECCSD

The ECCSD equations in Appendix A can be decomposed using

$$\begin{aligned} t_{ijkl} &= t_{ija} t_{kla} - t_{ika} t_{jla} + t_{ila} t_{kja} \\ V_{pqrs} &= \bar{V}_{pqa} V_{rsa}. \end{aligned} \quad (\text{B1})$$

Here, all the rank-3 tensors are antisymmetric in the first two indices. Since the singles part is unchanged, only the doubles contribution is presented here. The energy expectation value is

$$\begin{aligned} \langle - | e^{\hat{T}'} e^{-\hat{T}} \hat{H} e^{\hat{T}} | - \rangle_D &= \frac{1}{2} t_{kmtln} \bar{V}_{ija} V_{mna} t'_{ijb} t'_{klb} - \frac{1}{12} \bar{V}_{ima} V_{mna} t_{jkb} t_{lnb} (t'_{ikc} t'_{jlc} + t'_{ilc} t'_{jkc}) \\ &+ \frac{1}{4} \bar{V}_{mna} V_{ija} t_{klb} t_{mnb} (2t'_{ik} t'_{jl} - t'_{jc} t'_{klc}) - \frac{1}{6} \epsilon_{im} t'_{ija} t'_{kla} (2t_{jkb} t_{lmb} - t_{jmb} t_{klb}) \\ &+ \frac{1}{6} \bar{V}_{opa} V_{ija} t_{lmb} t_{npb} t_{ko} (4t'_{ik} t'_{jlc} t'_{nmc} - 2t'_{ik} t'_{jnc} t'_{lmc} - 12t'_{im} t'_{jnc} t'_{klc} - 12t'_{im} t'_{jlc} t'_{knc} \\ &\quad - 6t'_{im} t'_{jkc} t'_{lnc} - 3t'_{kn} t'_{ijc} t'_{lmc} - 2t'_{ij} t'_{klc} t'_{mnc} + t'_{ij} t'_{knc} t'_{lmc} + 6t'_{il} t'_{jm} t'_{kn}) \\ &+ \frac{1}{72} \bar{V}_{ija} V_{rsa} t_{nob} t_{psb} t_{klc} t_{mrc} \\ &\quad (12t'_{ijd} t'_{kld} t'_{mne} t'_{ope} - 6t'_{ijd} t'_{kld} t'_{mpe} t'_{noe} \\ &\quad + 36t'_{ijd} t'_{knd} t'_{lme} t'_{ope} + 36t'_{ijd} t'_{knd} t'_{loe} t'_{mpe} + 9t'_{ijd} t'_{mpd} t'_{lke} t'_{one} \\ &\quad - 72t'_{imd} t'_{jkd} t'_{lne} t'_{ope} + 72t'_{ipd} t'_{jnd} t'_{kle} t'_{moe} + 18t'_{imd} t'_{jld} t'_{kpe} t'_{one} \\ &\quad - 8t'_{ild} t'_{jpd} t'_{kme} t'_{noe} - 8t'_{ikd} t'_{jnd} t'_{lme} t'_{ope} - 2t'_{imd} t'_{jpd} t'_{kle} t'_{noe} \\ &\quad + 36t'_{ij} t'_{mn} t'_{lkd} t'_{opd} + 36t'_{ij} t'_{kp} t'_{lmd} t'_{ond} + 9t'_{ij} t'_{mp} t'_{lkd} t'_{ond} \\ &\quad + 24t'_{ik} t'_{jl} t'_{mod} t'_{npd} + 12t'_{ik} t'_{jl} t'_{mpd} t'_{nod} + 36t'_{ik} t'_{jp} t'_{mld} t'_{nod} - 18t'_{im} t'_{jp} t'_{lkd} t'_{nod} \\ &\quad + 144t'_{ik} t'_{ln} t'_{jmd} t'_{opd} + 144t'_{ik} t'_{mn} t'_{jld} t'_{pod} + 72t'_{il} t'_{kp} t'_{jmd} t'_{ond} - 72t'_{ik} t'_{lp} t'_{jmd} t'_{ond} \\ &\quad - 72t'_{ik} t'_{mp} t'_{jld} t'_{ond} - 12t'_{ij} t'_{kn} t'_{lp} t'_{mo} + 6t'_{ij} t'_{mp} t'_{ln} t'_{ko} + 144t'_{ik} t'_{jp} t'_{mo} t'_{ln} \\ &\quad - 72t'_{ik} t'_{jn} t'_{lp} t'_{mo} + 72t'_{ik} t'_{jn} t'_{lo} t'_{mp} + 36t'_{im} t'_{jp} t'_{lo} t'_{kn}). \end{aligned} \quad (\text{B2})$$

The particle number is

$$\langle \hat{N} \rangle_D = \frac{1}{6} t_{ijp} t_{klp} (3t'_{ijq} t'_{klq} + 2t'_{ilq} t'_{kjq}). \quad (\text{B3})$$

The matrix elements used to calculate excited state energies is

$$\begin{aligned} \langle - | \hat{d}_x e^{\hat{T}'} e^{-\hat{T}} \hat{H} e^{\hat{T}} \hat{d}_y^\dagger | - \rangle_D &= \bar{V}_{ija} V_{yoa} t_{xkb} t_{lob} (2t'_{il} t'_{jk} + t'_{ijc} t'_{klc}) + \\ &+ \frac{1}{2} \bar{V}_{ija} V_{yoa} t_{oxb} t_{klb} (2t'_{il} t'_{jk} + t'_{ijc} t'_{klc}) + \\ &+ \frac{1}{3} \bar{V}_{xia} V_{yoa} t_{klb} t_{mob} (2t'_{ikc} t'_{lmc} - t'_{imc} t'_{klc}). \end{aligned} \quad (\text{B4})$$

Finally, the expectation value required for calculating the superconducting gap is derived to be

$$\begin{aligned} \langle \hat{d}_x \hat{d}_y \rangle &= \frac{1}{8} t_{xia} t_{jka} t_{ylb} t_{mnb} (2t'_{in} t'_{jl} t'_{km} - t'_{kn} t'_{jm} t'_{il} - t'_{il} t'_{jkc} t'_{mnc} + \\ &\quad + 4t'_{im} t'_{jlc} t'_{knc} + 4t'_{il} t'_{jmc} t'_{knc}). \end{aligned} \quad (\text{B5})$$